Journal of Solid State Chemistry **149,** 327–332 (2000)
doi:10.1006/jssc.1999.8535, available online at http://www.idealibrary.com on IDEAL®

HRTEM Surface Profile Imaging of Superconducting $YBa_2Cu_4O_8$

Wuzong Zhou,*,[1] Yan Xin,† and David A. Jefferson*

*Department of Chemistry, University of Cambridge, Cambridge CB2 1EW, United Kingdom; and †Department of Materials Science and Metallurgy, University of Cambridge, Cambridge CB2 3QZ, United Kingdom

Received February 22, 1999; in revised form September 15, 1999; accepted October 22, 1999

Surface profile images have been recorded from high-Tc superconducting $YBa_2Cu_4O_8$ using high-resolution transmission electron microscopy. The surface regions are found to be relatively more stable than those of $YBa_2Cu_3O_7$. The stability of the double CuO chains in the vicinity of a crystal surface was found to depend on whether or not they were parallel or perpendicular to the surface in question. Possible mechanisms of the formation of both surface structures and near-surface defects are discussed.

INTRODUCTION

There are three main reasons why the surface chemistry of high-Tc superconducting compounds is currently of such great interest. First and probably most important, the physical properties of the superconductor, such as the transport critical currents, are affected greatly by the quality and true nature of the crystal surfaces both at the contact points and at grain boundaries within the superconductor itself (1). In particular, the surface structure directly affects the surface conductivity which is a crucial parameter in the development of microwave devices (2). Secondly, information regarding the surface structure of these compounds as well as the structure at the interface with a substrate is vital in producing high-quality superconducting thin films with predictable properties. Finally, the chemical stability of these materials within a variety of environments in most cases is dependent on their surface reactivity which in turn is determined by the surface structure present (3).

Over the last 12 years, many "state of the art" surface techniques, such as low-energy electron diffraction (LEED) (4) and scanning tunneling microscopy (STM) (5) were applied to study the surface features of high-Tc superconductors. These techniques suffer from the disadvantage that they require crystals with very clean and flat surfaces, and although excellent at revealing the surface arrangement, they give little information about the manner in which the surface relates to the underlying bulk structure. High-resolution transmission electron microscopy (HRTEM) was also used to investigate surface structures of various superconducting oxides and demonstrated several advantages when applied to these systems (6–14). For example, HRTEM can be used to study the surface of small crystallites of almost any morphology, and when employed in the profile-imaging mode, it gives direct atomic images of the topmost layer on the surface, together with its relationship to the structure beneath. The principal disadvantage with the profile-imaging technique in HRTEM is that the surface is veiwed only in projection: furthermore, the strong multiple scattering effects inherent in any electron-optical investigation make it necessary to determine the surface structure by trial and error, using structural models and image computations to simulate the image contrast using, for example, the multislice algorithm (15), and for an aperiodic feature such as a crystal surface the construction of these models may be a very time-consuming task. In addition, the chemical information which may be obtained using energy-dispersive X-ray spectroscopy (EDS) is limited both by the electron probe size, beam spreading, and current density. Nevertheless, the technique has shown its potential in systems of this type.

Several crystallographic surfaces of $YBa_2Cu_3O_7$, one of the most extensively investigated high-Tc superconductors, were studied using HRTEM and different amorphous coating layers were observed from the specimens crushed in different atmospheres (10). In a more recent case, it was found that such surface features had a marked effect on the magnetic properties of this material at temperatures below 10 K (16).

$YBa_2Cu_4O_8$ can be regarded as a derivative of the $YBa_2Cu_3O_7$ structure simply by introducing an extra CuO chain adjacent to the first one, thus forming a double CuO chain, shown schematically in Fig. 1. The number of Cu atoms coordinating to each oxygen atom in the CuO chains increases accordingly from two in $YBa_2Cu_3O_7$ to three in $YBa_2Cu_4O_8$. It is therefore interesting to compare the

[1]To whom correspondence should be addressed. Current address: School of Chemistry, University of St. Andrews, St. Andrews, Fife KY16 9ST, Scotland, U.K. Fax: 44-1334-463808. E-mail: wzhou@st-andrews.ac.uk.

0022-4596/00 $35.00

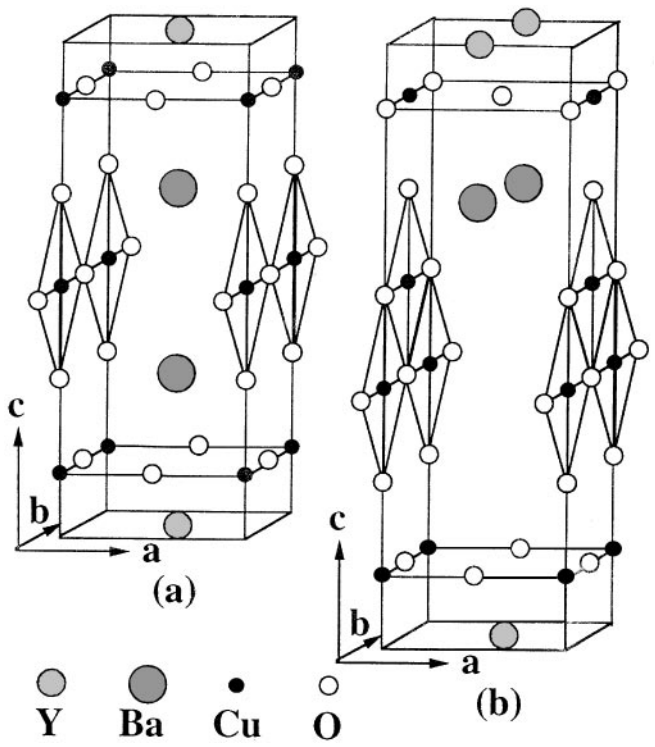

FIG. 1. Schematic drawings of the structures of (a) $YBa_2Cu_3O_7$ and (b) $YBa_2Cu_4O_8$.

HRTEM surface profile images from this compound to those from $YBa_2Cu_3O_7$. In a previous study, a very clean (001) surface of $YBa_2Cu_4O_8$ without any secondary phases nor decomposed amorphous coating was indeed observed (13). In this present work, further HRTEM profile images of various surfaces of $YBa_2Cu_4O_8$ are investigated and possible mechanisms for the formation of the surface structures and near-surface defects are discussed.

EXPERIMENTAL

The specimen of $YBa_2Cu_4O_8$ used in the present work was prepared by the same method as that described in a previous study (17). Initial characterization of the specimen was by X-ray powder diffraction (XRD), and the chemical compositions of individual particles were examined by EDS analysis fitted to a JEOL JEM-2010 electron microscope. For HRTEM studies, specimens were crushed in anhydrous methanol and deposited in a suspension onto Cu grids covered by a holey carbon film. After being allowed to dry in air, the specimen grid was then transferred into a JEOL JEM-4000EX-II electron microscope operating at 400 kV with objective lens parameters $C_s = 0.9$ mm and $C_c = 1.7$ mm and a point resolution of better than 0.17 nm. HRTEM images were recorded at a magnification of 500,000 $\times$. Structural models were constructed, and computer image simulations were performed using the "CERIUS" suite of programs developed by Cambridge Molecular Design Ltd.

RESULTS AND DISCUSSION

Both XRD and EDS studies showed that the majority phase in the sample was $YBa_2Cu_4O_8$. The Cu content in some particles did vary between 3 and 4, indicating a possible intergrowth of $YBa_2Cu_3O_7$ and $YBa_2Cu_4O_8$. The only significant impurity phase present was CuO.

Many HRTEM images showed $YBa_2Cu_4O_8$ crystallites with a very high degree of crystal perfection. However, defect structures, such as the intergrowth of $YBa_2Cu_4O_8$ with $YBa_2Cu_3O_7$, and rotation twinning of $YBa_2Cu_4O_8$ on the $\{001\}$ crystallographic planes, arising from an alternate arrangement of the double CuO chain along the *a* and *b* axes, were also observed in the HRTEM images. The formation mechanism of these defects were discussed previously (18–20). The impurity CuO crystallites were easily identified and showed no unusual features.

On all newly formed surfaces of $YBa_2Cu_3O_7$ (10) a thick (>5 nm) amorphous layer was found to be present after the sample had been crushed in air and was believed to arise from surface carbonate or oxide formation. Even when the crystal was crushed in an argon atmosphere, a disordered coating layer (ca. 2 nm) was still observed, indicating the inherent instability of the surface, but unlike the coating layer formed upon exposure to air, this disordered layer formed under argon was found to recrystallize after electron beam irradiation for several hours into the original structure of $YBa_2Cu_3O_7$, forming a perfectly clean surface. However, no substantial amorphous coating layer was observed on any surfaces of $YBa_2Cu_4O_8$ after the crystals were crushed in air, confirming the much greater surface stability of this phase. Figure 2a shows an initial HRTEM image of this compound when viewed down the *b* axis. The (100) surface is covered by a very thin (<1 nm) partly disordered metal oxide layer. After undergoing electron beam annealing for about 20 min, this layer crystallized and a relatively clean surface eventually appeared as shown in Fig. 2b.

The computer simulations indicate that, at the optimum focus and for a crystal thickness of less than 5 nm, the black dots in the image represent columns of cations and the elongated dots are in the positions of double CuO chains parallel to the electron beam direction as indicated in Fig. 4. This is the direction of the majority of the double CuO chains in this crystallite. However, the arrow in Fig. 2a indicates the position of a layer of double CuO chains which is perpendicular to the beam direction, constituting a twin defect. It may also be noted that the pairs of dark dots in the topmost atomic layer on the surface are at the positions of the end of CuO_2 planes (indicated by arrows in Fig. 2b) and that other dots in this surface layer are relatively dim and

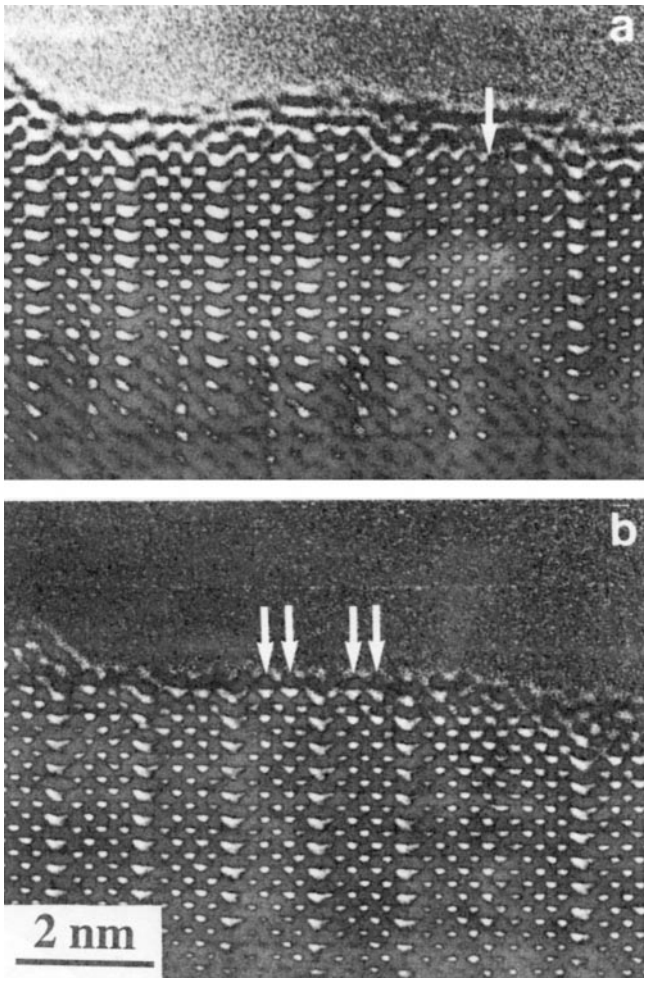

FIG. 2. (a) HRTEM image of $YBa_2Cu_4O_8$ viewed down the [010] direction, the arrow indicating a double CuO chain perpendicular to the beam direction; (b) HRTEM image from the same area as (a) after electron beam irradiation for about 20 min. The arrows indicate the CuO_2 planes.

less well-defined, indicating only a partial ordering of the atoms. When viewed in profile, this surface therefore shows "identations" which are spaced by $c/2$. If we consider the nature of the image contrast in Fig. 2b, it seems highly probable that the pairs of extra dark dots on the surface are most likely to be corresponding to Cu–O atomic columns.

The selective location of extra Cu atoms and the apparent deficiency of other metal atoms at the crystallite surfaces could arise from a consideration of the nature of the structure. If the (100) surface of the main part of the layer (excluding the double CuO chains) is terminated by a Y–Ba–O atomic layer, there are only oxygen anions at the ends of the CuO_2 planes and the oxygen coordination around Ba and Y is very much less than that in the bulk. This is particularly so as the double CuO chains are at a level slightly below the (100) surface plane. This unusual coordination state for Y and Ba cations at the surface could well induce the CuO_2 planes to accept two extra columns of Cu and oxygen atoms, as shown in Fig. 3a. In these columns the coordination of the Cu atoms by oxygen is reduced from 4 to 3, but the increase in energy resulting from this is presumably more than offset by that resulting from the increase in Ba and Y coordination. It is worth noting that this type of structural feature was never observed in $YBa_2Cu_3O_7$, in which the distance between two BaO layers is much smaller due to the presence of only a single CuO chain and the reduction in the coordination of surface Ba and Y is not so marked.

When the double CuO chain is perpendicular to the surface (as indicated by the arrow in Fig. 2a), this small surface region can be considered as a local (010) rather than (100) surface and oxygen anions appear at the end of the CuO chains as well as the si1tes in the CuO_2 planes in any terminal plane (Fig. 3b). the terminating plane at the surface is then composed exclusively of Cu and oxygen atoms, and the coordination requirements are more nearly satisfied. Consequently, the profile view of the final surface shows no indentations.

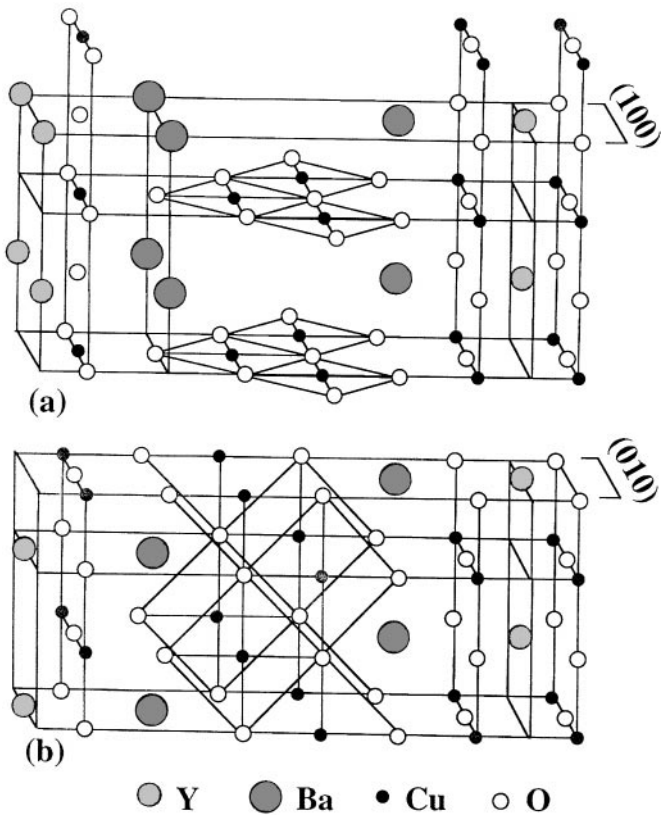

FIG. 3. (a) A structural model for the recrystallized (100) surface of $YBa_2Cu_4O_8$ shown in Fig. 2b. (b) The (010) surface of the compound terminated with the Y–Ba–O layer.

To confirm the surface model of Fig. 3a, computer image simulations were performed. The surface model for the calculation was built up as follow: A $10a \times b \times c$ superlattice with $a = 3.8411$, $b = 0.38718$, and $c = 2.7240$ nm based on the $YBa_2Cu_4O_8$ subcell was created and a facet parallel to the *bc* plane at the position $a = 0.5$ was set in this supercell. All the atoms outside this facet were removed, leaving a flat (100) surface with a terminating plane containing Y, Ba, and oxygen atoms. Extra Cu and oxygen atoms were then added to extend the CuO_2 planes as shown in Fig. 3a. The electron microscope parameters used in the calculations were as follows: accelerating voltage, 400 kV; coefficient of spherical aberration (C_s), 0.9 mm; defocus spread (assuming a chromatic aberration coefficient (C_c) of 1.7 mm and an intrinsic energy spread of 1.5 eV), 10 nm; and beam divergence, 1.3 mrad. The simulated images are shown in Fig. 4. Except for the weak and disordered dots within each indentation, the details of the observed image contrasted in Fig. 2b were reproduced.

Replacing Cu atoms in the extra columns on the surface Y or Ba not only makes no sense in structural chemistry but also gives unexpected larger and darker dots in the simulated images. Removing oxygen ions from these columns results in a slight reduction of darkness of the surface dots, but still gives a reasonably good image matching. The proposed model shown in Fig. 3a is therefore a good approach to the real surface structure in which the occupation factor for the oxygen sites in the surface Cu–O columns may be reduced.

The different nature of the (100) and (010) surfaces discussed above was also observed from many other images. Figure 5 shows a typical HRTEM surface profile image of $YBa_2Cu_4O_8$ when viewed down the *a* axis. This crystallite is perfect with no visible intergrowths with $YBa_2Cu_3O_7$, rota-

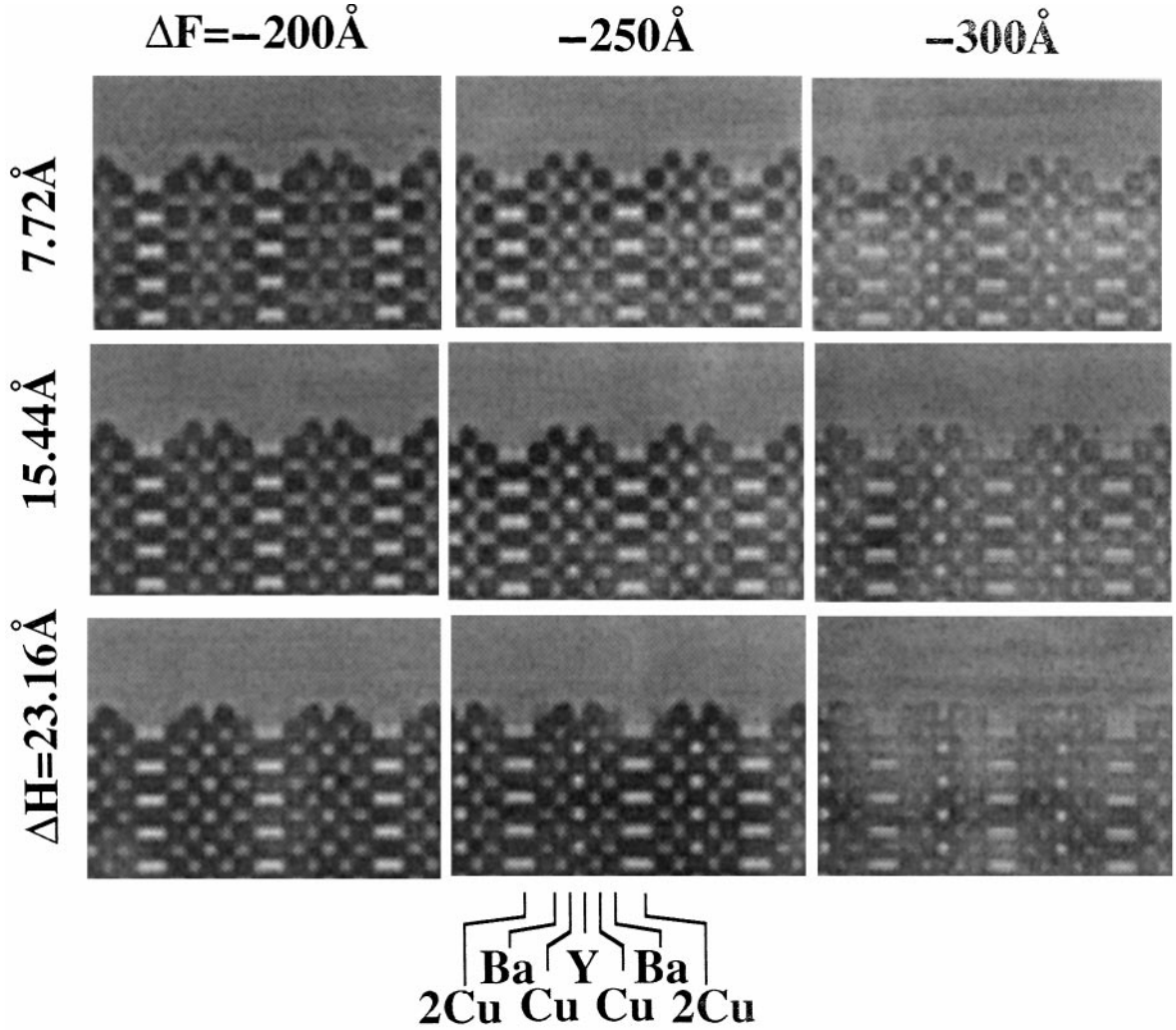

FIG. 4. Computer simulated images of the surface of Fig. 2b using the surface model of Fig. 3a. ΔH, specimen thicknesses; ΔF, lens defocusses. Positions of the atomic layers are indicated by cations.

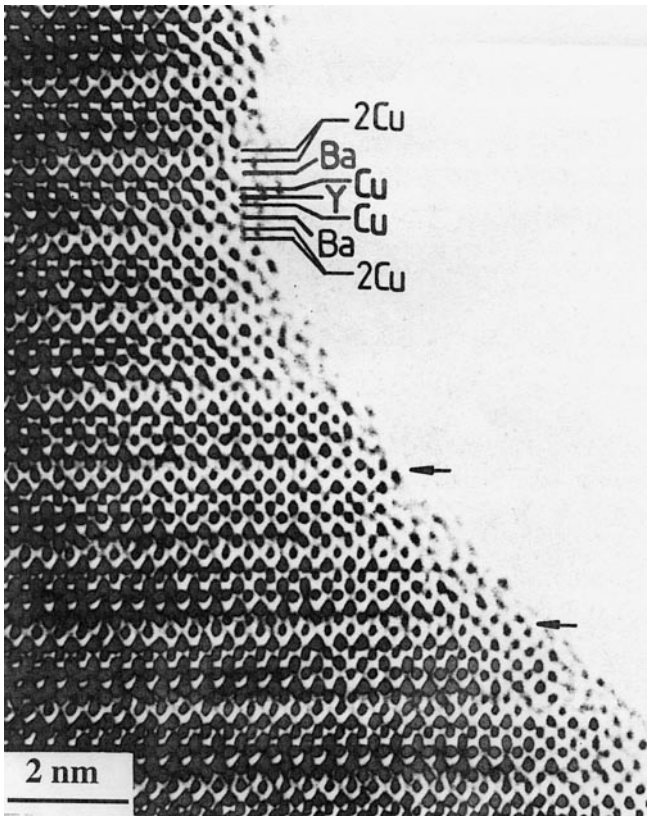

FIG. 5. HRTEM profile image of $YBa_2Cu_4O_8$ viewed down the [100] direction. The corresponding arrangement of cations along the *c* axis are indicated.

tion twins, or other defects. By comparison with computer image simulations, every atomic layer can be correlated with the observed dark dots, as marked in the image.

The upper part of Fig. 5 constitutes an approximately (010) surface with one or two atomic layers decomposed, similar to that illustrated in Fig. 2a. In contrast, the lower part of Fig. 5 approximates to a (015) surface. Some part of the actual crystallite surface is made up of steps comprising alternate small regions of the (001) and (010) planes, with some atoms in an apparently disordered array filling each step. This is very similar to the (11*l*) surface of $Tl_2Ba_2Ca_2Cu_3O_{10}$ (11). A closer examination of the surface steps in Fig. 5, considered in relation to the assignment of dark dots referred to above, reveals that the (001) surface plane is either at the level of a BaO layer or a double CuO chain, and the (010) surface is usually terminated with a Y–Ba–O atomic layer. It is particularly interesting to note that the double CuO chains can extend to the level of the (010) surface without detectable distortion or decomposition, as indicated by arrows.

A stepped surface of this type was not observed in HRTEM images when crystallites were viewed down the *b* axis. Figure 6 shows one such image where an approximate (1 0 15) surface is present. In this image, the layers of elongated black dots corresponding to the double CuO chains viewed "end on" invariably do not extend to the surface. Instead, these double atomic layers appear to become single atomic layers near the surface, as indicated by the arrows, and the surface structure is distorted. This coexistence of double and single CuO chains in the same layer is unlikely to occur inside the crystal because it will result in very high lattice strain and a dislocation with a Burgers vector parallel to the incident beam must be introduced. In the case of (10*l*) surfaces (when *l* is large), this type of strain appears to be released quite easily by surface relaxation.

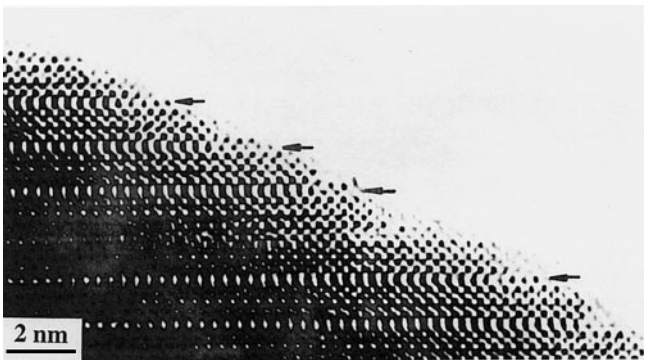

FIG. 6. HRTEM image of $YBa_2Cu_4O_8$ viewed down the [010] zone axis, an approximate (1 0 15) surface being present. The arrows indicate the double CuO chains which are parallel to the beam direction and turn to single atomic layers near the surface.

In summary, a variety of surface profile images were obtained from superconducting $YBa_2Cu_4O_8$ using the HRTEM technique. The surface stability of this material is clearly higher than that of $YBa_2Cu_3O_7$. The stability of the double CuO chains which distinguish this structure in the region of the surface appears to depend on whether they lie perpendicular or parallel to the surface. Consequently, although the (100) and (010) planes containing Y, Ba, and oxygen atoms in this compound are very similar except for a differing oxygen content, the corresponding two surfaces, in addition to surfaces of the form (10*l*) and (01*l*), have significantly different surface structures and grain boundary properties.

ACKNOWLEDGMENT

The authors thank Prof. C. J. Humphreys for helpful suggestions on the explanation of the surface structures.

REFERENCES

1. D. Dimos, P. Chaudharri, J. Mannhart, and F. K. Legoues, *Phys. Rev. Lett.* **61,** 219 (1988).

2. S. S. Laderman, R. C. Taber, R. D. Jacowitz, J. L. Moll, C. B. Eom, T. L. Hylton, A. F. Marshall, T. H. Geballe, and M. R. Beasley, *Phys. Rev. B* **43,** 2922 (1991).
3. A. Crossley, P. R. Graves, and S. Myhra, *Physica C* **176,** 106 (1991).
4. N. Brooks, A. Viescas, P. D. Johnson, J. P. Remeika, A. S. Cooper, and N. V. Smith, *Surf. Sci.* **203,** L627 (1988).
5. M. D. Kirk, J. Nogami, A. A. Baski, D. B. Mitzi, A. Kapitulnik, T. H. Geballe, and C. F. Quate, *Science* **242,** 1673 (1988).
6. H. W. Zandbergen, P. Groen, G. van Tendeloo, J. van Landuyt, and S. Amelinckx, *Solid State Commun.* **66,** 397 (1988).
7. W. Zhou, D. A. Jefferson, and W. Y. Liang, *Surf. Sci.* **209,** 444 (1989).
8. W. Zhou, D. A. Jefferson, W. Y. Liang, A. Soeta, T. Kamo, and S. P. Matsuda, *Physica C* **202,** 335 (1992).
9. H. W. Zandbergen, *Physica C* **194,** 287 (1992).
10. W. Zhou, D. A. Jefferson, and W. Y. Liang, *Supercond. Sci. Technol.* **6,** 81 (1993).
11. W. Zhou, D. A. Jefferson, and W. Y. Liang, *Surf. Sci.* **310,** 52 (1994).
12. W. Zhou, A. Asab, I. Gameson, D. A. Jefferson, and P. P. Edwards, *Physica C* **248, 1** (1995).
13. Y. Xin, W. Zhou, and C. J. Huphreys, *Physica C* **249,** 319 (1995).
14. W. Zhou, *J. Supercond.* **9,** 311 (1996).
15. J. M. Cowley and A. F. Moodie, *Acta. Crystallogr.* **10,** 609 (1957).
16. C. Panagopoulos, W. Zhou, N. Athanassopoulou, and J. R. Cooper *Physica C* **269,** 157 (1996).
17. J. S. Ho, C. T. Chang, R. S. Liu, and P. P. Edwards, *Appl. Phys. Lett.* **58,** 2426 (1991).
18. B. Domenges, M. Hervieu, B. Raveau, J. Karpinski, E. Kaldis, and S. Rusiecki, *J. Solid State Chem.* **93,** 316 (1991).
19. K. Yamaguchi, T. Miyatake, T. Takata, S. Gotoh, N. Koshizuka, and S. Tanaka, *Jpn. J. Appl. Phys.* **28,** L1942 (1989).
20. T. Krekels, G. Vantendeloo, S. Amelinckx, D. M. Deleeuw, and M. Dekraan, *Physica C* **169,** 457 (1990).